Progress In Electromagnetics Research, PIER 72, 159–185, 2007

ON REDUCING THE PHASE ERRORS IN THE APERTURE OF A RADIAL WAVEGUIDE PIN-FED NON-RESONANT ARRAY ANTENNA

L. Pazin and Y. Leviatan

Department of Electrical Engineering
Technion — Israel Institute of Technology
Haifa 32000, Israel

Abstract—With a proper design, the aperture field of a conventional radial waveguide pin-fed non-resonant array antenna (RWPFAA) can be rendered equiphase at a given central frequency. However, when the operating frequency deviates from this central frequency, the aperture field will exhibit an undesired conical phase error. To alleviate this problem, we propose a novel design in which the frequency-dependent aperture phase error distribution is rendered serrated. The gain and side-lobes of an RWPFAA with serrated phase error distributions are studied by resorting a simple model of a line source as well as a more representative model of a circular aperture. The theoretical results are supplemented by numerical data. Schemes of RWPFAAs comprising two and three sections, which render the phase error distribution in the antenna aperture serrated, are suggested.

1. INTRODUCTION

Over the last years, several types of the radial-waveguide (radial-line) pin-fed non-resonant circular array antenna (RWPFAA) have been suggested. Antennas of this kind are attractive for modern terrestrial and satellite communication systems due to their low profile and high efficiency. This first antenna was proposed by Kraus in 1964 and studied thereafter by Carver [1]. In this RWPFAA, the pin-fed radiating elements were long helices. Similar RWPFAAs, but with low profile helical and curl radiating elements, were later suggested by Nakano et al. [2, 3]. At about the same time, Haneishi and Saito described an RWPFAA with microstrip radiating elements [4]. More recent designs of RWPFAAs with different radiating characteristics can be found in [5–7]. However, these antennas are narrowband and

may not satisfy the wideband gain and side-lobe level requirements of modern communication antennas (see, for example, [8]). For example, the antenna described in [2] has no more than 3% bandwidth, in which the gain G is larger than $0.7G_{\max}$, even though the radiating elements that were used were all wideband. This drawback of the RWPFAA is mainly due to the inherent frequency-dependent conical phase error in the array, where the radiating elements are excited by a traveling wave in the radial waveguide. As was shown in [9], the phase error increases as the operating frequency deviates from the one at which the array was adjusted for in-phase aperture excitation. This phase error not only severly reduces the antenna gain factor, but it also increases the antenna side-lobes. An approach to decreasing the phase error effect in a radial waveguide array antenna was suggested in [10]. The idea was to reduce the phase error by exciting the radial waveguide not at its center but rather through an annular gap in its bottom wall. In this way, the frequency-dependent phase error distribution in the antenna aperture is rendered serrated and its effect on the radiation pattern becomes less pronounced. The purpose of our paper is to further extend the theory of this idea using simple, yet representative, models.

The paper is organized as follows. Section 2 presents a study of the crude, but closely analogous, model of a line source with different types of piecewise-linear phase distributions. In Section 3, the analysis is extended to a circular aperture model of the circular array antenna. Schemes of modified RWPFAAs, comprising two, three, and four sections, which render the phase error distribution in the antenna aperture serrated, are also given in Section 3. Finally, some concluding remarks are given in Section 4.

2. LINE SOURCE MODELS

2.1. Line Source with a Linear Symmetric Phase Distribution

Following [11], we consider an x-directed line source of length L centered about the origin. The current distribution along the line source is assumed to be uniform, of unit amplitude, and its phase is assumed to be linear and symmetric about the source midpoint. In terms of a normalized coordinate $\mathcal{x} = x/(L/2)$, the current of this line source is given by $I(\mathcal{x}) = \exp[j\Phi(\mathcal{x})]$, where

$$\Phi(\mathcal{x}) = \begin{cases} -\beta\mathcal{x} & -1 \le \mathcal{x} \le 0 \\ \beta\mathcal{x} & 0 \le \mathcal{x} \le 1. \end{cases} \tag{1}$$

Here, β, $|\beta| \leq 2\pi$, is the normalized phase constant which can be interpreted as the phase at the line source ends. For analogy with the frequency dependence of the aperture phase distribution in the case of the RWPFAA [9], β is assumed to be linearly dependent on the frequency and we let $\beta = (\pi L/\lambda_0)\nu$. Here, λ_0 denotes the wavelength corresponding to f_0, where f_0 is the central frequency at which the phase of the current along the line source is zero. Also, $\nu = (f - f_0)/f_0$ is the relative frequency deviation of the operating frequency f from the central one. Clearly, the larger the deviation from the central frequency the larger β.

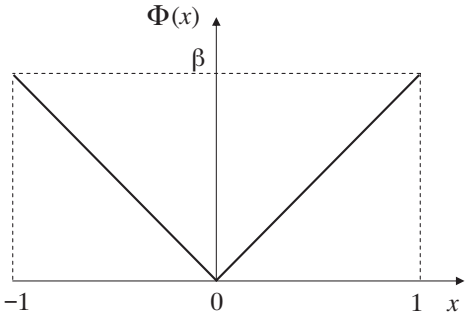

Figure 1. Linear symmetric phase distribution along the line source.

A plot of $\Phi(x)$ is shown in Fig. 1. For this line source, the space factor $SF(u)$ can be written as

$$SF(u) = 0.5 \int_{-1}^{1} I(x) \exp(-jux)\, dx = 0.5 \int_{-1}^{1} \exp[j\Phi(x)] \exp(-jux)\, dx$$
$$= 0.5 \left[\int_{-1}^{0} \exp(-j\beta x) \exp(-jux) + \int_{0}^{1} \exp(j\beta x) \exp(-jux)\, dx \right]. \tag{2}$$

Here, $u = \pi(L/\lambda)\sin\theta$ is a generalized angular coordinate, where λ is the operating wavelength and θ is the angle measured from z axis (broadside direction) in the xz plane. For simplicity, we consider only the $z > 0$ half plane. Carrying out the integrals in (2) analytically, we arrive at

$$SF(u) = \frac{u \sin u \cos\beta - \beta \sin\beta \cos u}{u^2 - \beta^2} + j\, \frac{u \sin\beta \sin u + \beta \cos u \cos\beta - \beta}{u^2 - \beta^2}. \tag{3}$$

A quantity of interest in this study is the normalized space factor $SF_{\rm n}(u) = |SF(u)|/|SF(0)|$, where

$$|SF(0)| = \frac{\sqrt{2(1-\cos\beta)}}{\beta} \tag{4}$$

is the magnitude of the space factor in the broadside direction. Plots

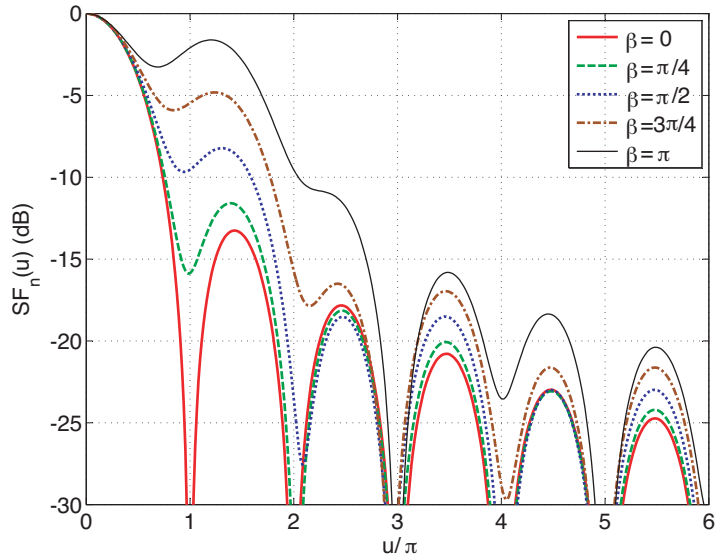

Figure 2. Plots of the normalized space factor of a line source with uniform amplitude distribution and linear symmetric phase distribution for different values of the phase constant β.

of $SF_{\rm n}(u)$ for various values of the phase constant β are shown in Fig. 2. Note that the side-lobes (especially, the first side-lobe) are higher when the phase constant β is larger. Note also that as β gets larger, the first null is filled up and a pedestal is formed around the main lobe. This latter phenomenon of the filling of the first null occurs even for small values of the phase constant β. To illustrate this, we assume that $\beta \ll 1$, in which case (3) can be approximated by

$$SF(u) = \frac{\sin u}{u} + j\beta \int_0^1 x \cos ux \, dx = \frac{\sin u}{u} + j\beta F_1(u). \tag{5}$$

The $\sin u/u$ term (real component) on the right hand side of (5) is the well-known space factor for a uniformly and in-phase excited line

source, and $j\beta F_1(u)$ is a correction term due to the deviation of the phase from the uniform one. Here,

$$F_1(u) = \frac{u \sin u + \cos u - 1}{u^2}. \tag{6}$$

Plots of $F_1(u)$ and of the space factor main term $\sin u/u$ are superimposed in Fig. 3 and show clearly that the value of the correction term in the direction of the first null of the main term is not zero.

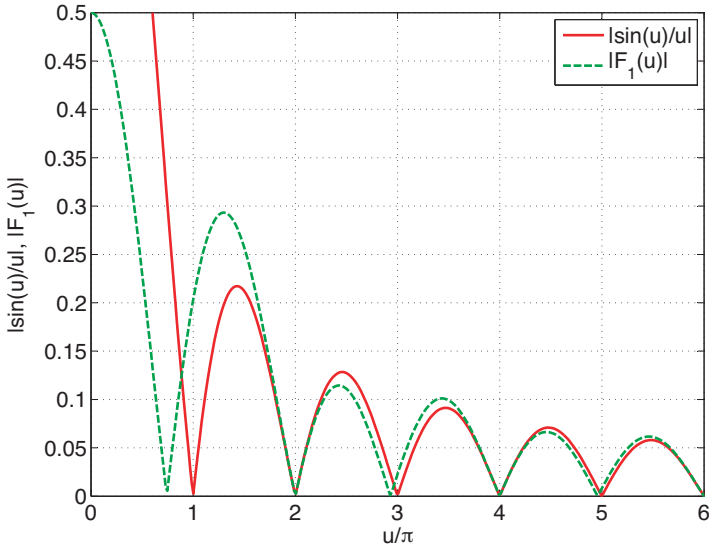

Figure 3. Plot of the function $F_1(u)$.

Another quantity of interest is the gain factor of the line source, which is the ratio between the actual gain of the antenna and the gain of the same antenna assuming its aperture amplitude and phase are uniform. Expressing the gain factor g in terms of the space factor SF, we readily find that

$$g = |SF(0)|^2. \tag{7}$$

From the broadening of the main lobe of $SF_{\rm n}(u)$ seen in Fig. 2 one can easily infer that g decreases as β increases. An expression for the gain factor of the line source readily follows from (4). We have

$$g = \frac{2(1 - \cos\beta)}{\beta^2}. \tag{8}$$

Values of g are presented for various values of β in Table 1.

Table 1. Gain factor of the uniformly excited line source with linear symmetric phase distribution.

β	0	$\pi/4$	$\pi/2$	$3\pi/4$	π
$g\,(\mathrm{dB})$	0	-0.22	-0.91	-2.11	-3.92

2.2. Line Source with a Regularly Serrated Phase Distribution

Anticipating that the negative effect of the linear symmetric phase distribution on the space factor will be reduced if the maximal phase deviation from the zero along the line is decreased, we examine the case of a line source with different regularly serrated phase distributions. Serrated phase distributions are characteristics of the phase error distributions in the aperture of array antennas designed for wide-band operation such as the radial line slot antenna proposed in [10]. The two simplest kinds of the regularly serrated phase distribution under consideration are shown in Fig. 4. The first is a saw-tooth phase distribution given by

$$\Phi(x) = \begin{cases} \beta x + \beta & -1 \le x \le -0.5 \\ -\beta x & -0.5 \le x \le 0 \\ \\ \beta x & 0 \le x \le 0.5 \\ -\beta x + \beta & 0.5 \le x \le 1. \end{cases} \tag{9}$$

The second is a shark-tooth phase distribution given by

$$\Phi(x) = \begin{cases} -\beta x - \beta/2 & -1 \le x \le -0.5 \\ -\beta x & -0.5 \le x \le 0 \\ \\ \beta x & 0 \le x \le 0.5 \\ \beta x - \beta/2 & 0.5 \le x \le 1\,. \end{cases} \tag{10}$$

For both types of the serrated phase distribution and for a given value of β, the maximum phase along the line-source is half that of the previously considered line source model. In this case, for the line source model with a uniform amplitude distribution, the values of the radiated power are equal to each other for all sections obtained from the regular serration of the phase distribution. The space factor of the line source

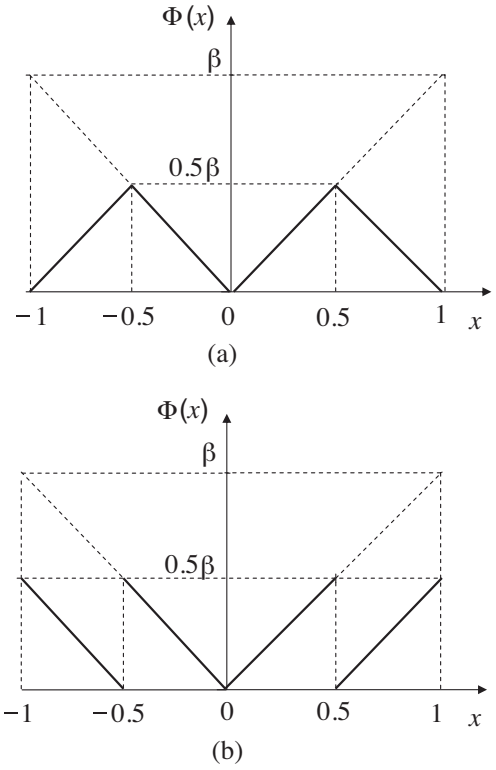

Figure 4. Serrated phase distributions along the line source: (a) saw-tooth phase distribution; (b) shark-tooth phase distribution.

for the case of the saw-tooth phase distribution can be written as

$$\begin{aligned} SF(u) =& 0.5\left[\exp(j\beta)\int_{-1}^{-0.5}\exp(j\beta x)\exp(-jux)\,dx\right. \\ &+\int_{-0.5}^{0}\exp(-j\beta x)\exp(-jux)\,dx \\ &+\int_{0}^{0.5}\exp(j\beta x)\exp(-jux)\,dx \\ &\left.+\exp(j\beta)\int_{0.5}^{1}\exp(-j\beta x)\exp(-jux)\,dx\right]. \end{aligned} \tag{11}$$

Similarly, the space factor of the line source with the shark-tooth phase distribution can be written as

$$\begin{aligned} SF(u) =& 0.5\Bigg[\exp(-j\beta/2)\int_{-1}^{-0.5}\exp(-j\beta\mathcal{x})\exp(-ju\mathcal{x})\,d\mathcal{x} \\ &+\int_{-0.5}^{0}\exp(-j\beta\mathcal{x})\exp(-ju\mathcal{x})\,d\mathcal{x} \\ &+\int_{0}^{0.5}\exp(j\beta\mathcal{x})\exp(-ju\mathcal{x})\,d\mathcal{x} \\ &+\exp(-j\beta/2)\int_{0.5}^{1}\exp(j\beta\mathcal{x})\exp(-ju\mathcal{x})\,d\mathcal{x}\Bigg]. \end{aligned} \tag{12}$$

Explicit expressions for the above two space factors can be found by carrying out the integrals in (11) and (12) analytically. However, because these expressions are rather bulky, they will not be presented herein.

The values of the normalized space factor in the other directions for the two serrated phase distribution under consideration can be derived by carrying out the integrations in (11) and (12) numerically. Two sets of plots of the normalized space factors are shown in Fig. 5. They are for the same values of the phase constant β used earlier. The plots clearly show that, in both of the serrated phase distribution cases, the side-lobe levels do not increase now, for the circular aperture model, as fast when the phase constant β increases. Moreover, while in these cases the uniform-phase case side-lobe structure is also distorted, this distortion takes other forms. Specifically, as can be seen in Fig. 5(a), for the saw-tooth phase distribution, the second null is gradually filled up resulting in a rising of a wide side-lobe that extend over the region of the second and third uniform-phase case side-lobes. At the same time, as can be seen in Fig. 5(b), for the shark-tooth phase distribution, the third null is gradually filled up resulting in a rising of a wide side-lobe, though of slightly lesser level, that overlaps the region of third and fourth uniform-phase case side-lobes. The phenomenon of the filling of the nulls occurs even for small values of the phase constant β. To illustrate this, we assume that $\beta \ll 1$, in which case (11) can be

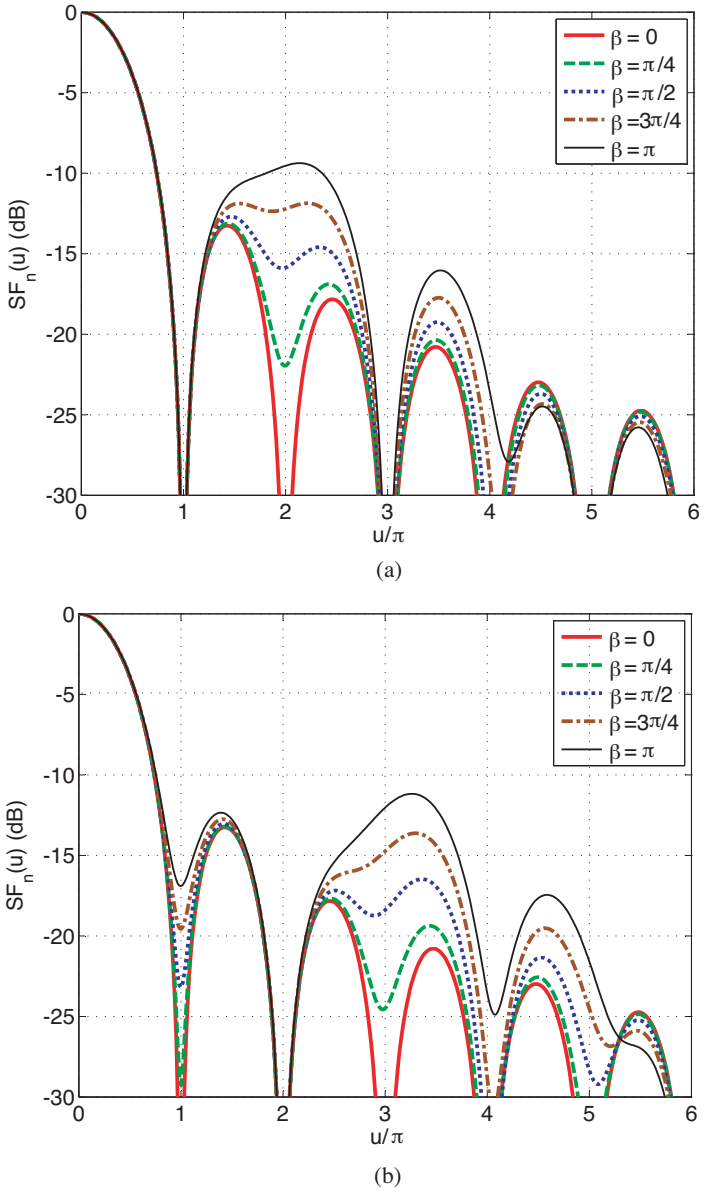

Figure 5. Plots of the normalized space factor of a line source with uniform amplitude distribution and serrated phase distribution for different values of the phase constant β: (a) saw-tooth phase distribution; (b) shark-tooth phase distribution.

approximated by

$$SF(u) = \frac{\sin u}{u} + j\beta F_2(u) \tag{13}$$

where

$$\begin{aligned} F_2(u) &= \int_0^{0.5} x \cos ux \, dx - \int_{0.5}^{1} x \cos ux \, dx + \int_{0.5}^{1} \cos ux \, dx \\ &= \frac{2\cos 0.5u - \cos u - 1}{u^2}. \end{aligned} \tag{14}$$

The $j\beta F_2(u)$ term in (13) is the angle-dependent correction term due to the deviation of the saw-tooth phase distribution from the uniform one. Similarly, for $\beta \ll 1$, the space factor given by (12) can be approximated by

$$SF(u) = \frac{\sin u}{u} + j\beta F_3(u) \tag{15}$$

where

$$F_3(u) = \int_0^{1} x \cos ux \, dx - 0.5 \int_{0.5}^{1} \cos ux \, dx = \frac{u \sin u + \cos u - 1}{u^2}. \tag{16}$$

The $j\beta F_3(u)$ term in (15) is the angle-dependent correction term due to the deviation of the shark-tooth phase distribution from the uniform one. In Fig. 6, plots of functions $F_2(u)$ and $F_3(u)$ and of the space factor main term $\sin u/u$ are superimposed. Specifically, for the saw-tooth phase distribution, Fig. 6(a) shows that the center of the first side-lobe of the function $F_2(u)$ coincides with the location of the second null of the main term $\sin u/u$ leading to a filling of this null and to a formation of a much wider first side-lobe. Similarly, for the shark-tooth phase distribution, Fig. 6(b) shows that the locations of the odd nulls do not coincide with the locations of the nulls of the main term $\sin u/u$. The resulting rising and substantial widening of the second wide side-lobe can be seen in Fig. 5(b).

The gain factor for both types of the serrated phase distribution can be obtained from the values of the respective space factors in the broadside direction via (7). From (11) and (12), it is found that for both of the regularly serrated phase distributions, the magnitude of the space factors is the same and given by

$$|SF(0)| = \frac{2\sqrt{2(1 - \cos 0.5\beta)}}{\beta}. \tag{17}$$

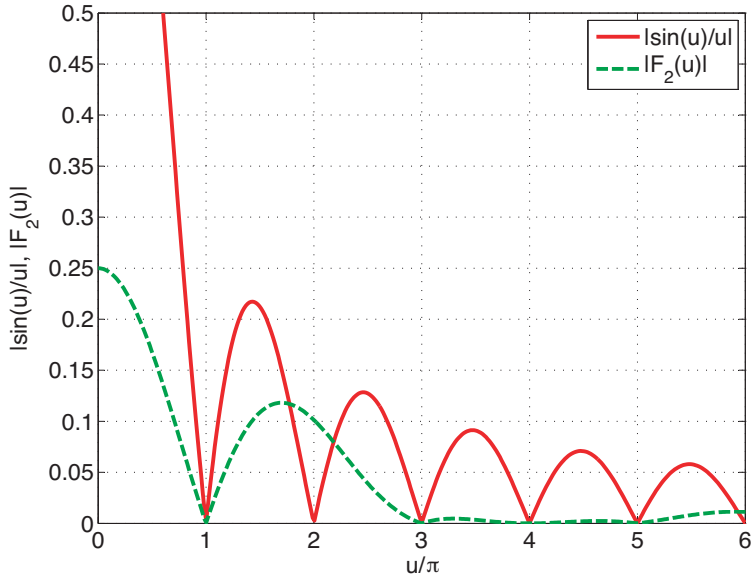

(a)

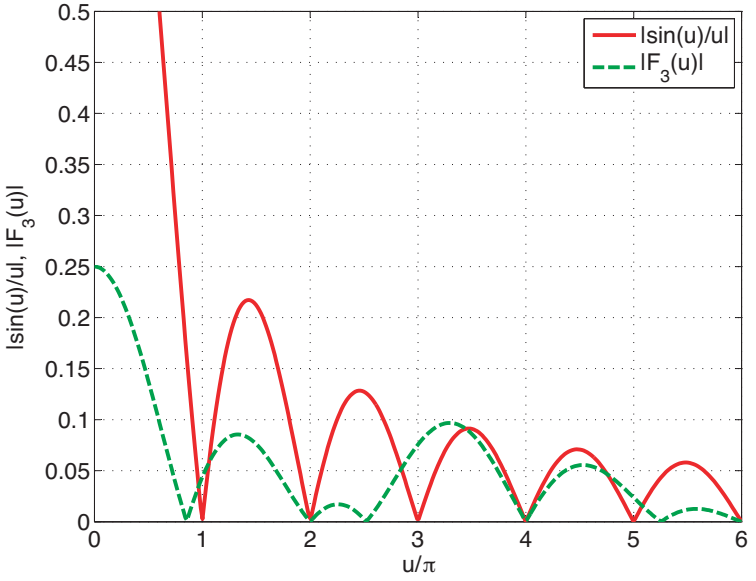

(b)

Figure 6. Plots of the functions (a) $F_2(u)$ and (b) $F_3(u)$.

Then, we have

$$g = \frac{8(1 - \cos 0.5\beta)}{\beta^2}. \tag{18}$$

Values of the gain factor g are presented for various values of β in Table 2. A comparison of Table 2 with Table 1 shows indeed that the decrease in gain with increasing β when the phase is serrated is markedly less than that occurring when the phase is linear.

Table 2. Gain factor of the uniformly excited line source with regularly serrated phase distributions.

β	0	$\pi/4$	$\pi/2$	$3\pi/4$	π
g (dB)	0	-0.06	-0.22	-0.51	-0.91

3. CIRCULAR APERTURE MODELS

3.1. Circular Aperture with a Conical Phase Distribution

Consider next a circular aperture of diameter D centered about the origin. The field distribution in the aperture is assumed to be uniform, of unit amplitude, and its phase is assumed to be conical and symmetric about the aperture center. In terms of a normalized radial coordinate $r = \rho/(D/2)$, where ρ is the radial coordinate of a point in the aperture, the field of this circular aperture is given by $E(r) = \exp[j\Phi(r)]$. Here,

$$\Phi(r) = \beta r \tag{19}$$

where β, $|\beta| \leq 2\pi$, is a normalized phase constant. Such phase distribution is characteristic of the phase error distribution in the aperture of RWPFAA [9]. For the RWPFAA, β is given by

$$\beta = (\pi D/\lambda_0)\nu \tag{20}$$

where λ_0 denotes as before the wavelength corresponding to the central frequency f_0 at which the field over the aperture is equiphase and its phase is zero, and $\nu = (f - f_0)/f_0$ denotes, as before, the relative frequency deviation of the operating frequency f from the central one. A plot of $\Phi(r)$ is shown in Fig. 7.

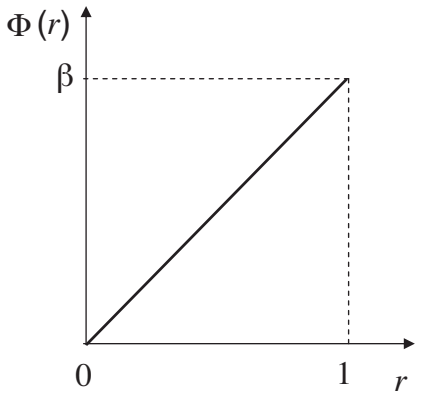

Figure 7. Phase distribution along the circular aperture radius (conical phase distribution).

Expression for the space factor $SF(u)$ of the circular aperture can be written as

$$SF(u) = 2\int_0^1 E(r)J_0(ur)r\,dr = 2\int_0^1 \exp(j\beta r)J_0(ur)r\,dr\,. \qquad (21)$$

Here, J_0 is the Bessel function of the first kind of zero order, $u = \pi(D/\lambda)\sin\theta$ is a generalized angular coordinate, where λ is the operating wavelength, and θ is the angle measured from z axis (broadside direction). In general, the integral in (21) cannot be carried out analytically except for the broadside direction ($u = 0$).

Figure 8 shows a plot of the normalized space factor $SF_n(u)$ obtained by carrying out the integration in (21) numerically. Plots shown are for various values of the phase constant β. Note that the phenomenon of the filling of the first null occurs as before even for small values of the phase constant β. To illustrate this, we assume that $\beta \ll 1$, in which case (21) can be approximated by

$$SF(u) = \Lambda_1(u) + j\beta F_4(u) \qquad (22)$$

where the Lambda function $\Lambda_1(u)$ (real component) is the well-known space factor for a uniformly and in-phase excited circular aperture, and $j\beta F_4(n)$ is a correction term due to the deviation of the phase from

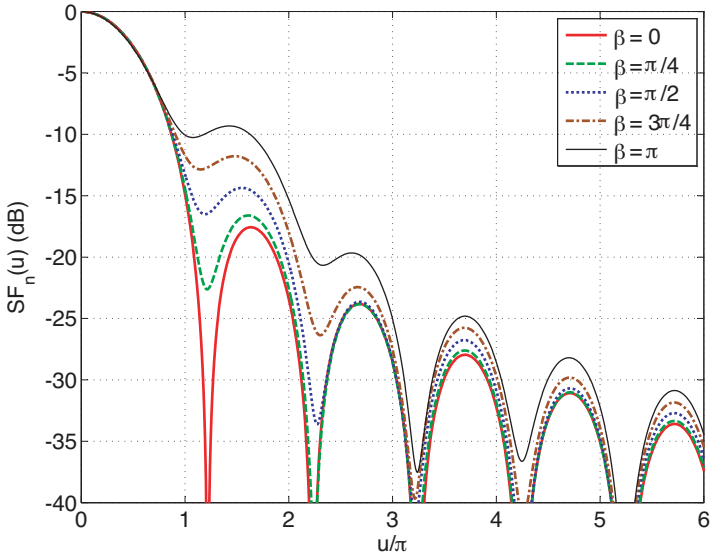

Figure 8. Plots of the normalized space factor of a circular aperture with uniform amplitude distribution and conical phase distribution for different values of the phase constant β.

the uniform one. Here

$$F_4(u) = 2\int_0^1 J_0(ur)r^2\,dr. \tag{23}$$

Plots of the function $F_4(u)$ and of the space factor main term $\Lambda_1(u)$ are superimposed in Fig. 9. They show clearly that the value of the correction term in the direction of the first null of the main term is not zero. Like in the line source case, a decrease in the gain factor g with increasing β, as can be observed in Fig. 8, is also a characteristic of the circular aperture case.

Finally, we turn to evaluate the gain factor of the circular aperture. Towards this end, one should again determine the value of the respective space factor in the broadside direction. It is readily found from (21) that in this case

$$|SF(0)| = \frac{2}{\beta^2}\sqrt{\beta^2 + 2(1 - \cos\beta - \beta\sin\beta)}. \tag{24}$$

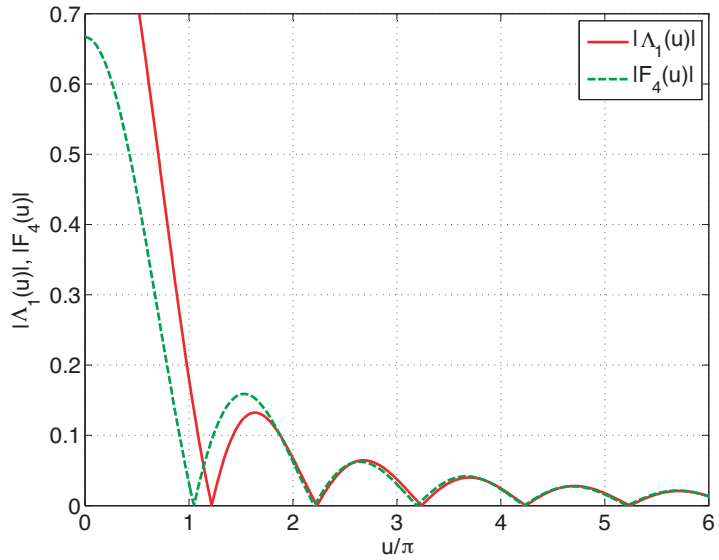

Figure 9. Plot of the function $F_4(u)$.

Then, by substituting (24) into (7), we arrive at

$$g = \frac{4}{\beta^4}\left[\beta^2 + 2(1 - \cos\beta - \beta\sin\beta)\right]. \tag{25}$$

Values of the gain factor are presented for various values of β in Table 3.

Table 3. Gain factor of the uniformly excited circular aperture with conical phase distribution.

β	0	$\pi/4$	$\pi/2$	$3\pi/4$	π
g (dB)	0	-0.15	-0.6	-1.36	-2.44

3.2. Circular Aperture with a Regularly Serrated Phase Distribution

Let us now examine the case of a circular aperture with uniform amplitude distribution and regularly serrated phase distribution. The two simplest cases of regularly serrated phase distributions are shown in Fig. 10. The first is a saw-tooth phase distribution along the circular

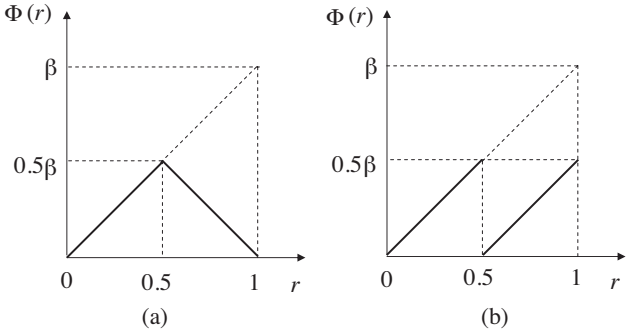

Figure 10. Serrated phase distributions along the circular aperture radius: (a) saw-tooth phase distribution; (b) shark-tooth phase distribution.

aperture radius given by the piecewise linear function

$$\Phi(r) = \begin{cases} \beta r & 0 \le r \le 0.5 \\ -\beta r + \beta & 0.5 \le r \le 1\,. \end{cases} \tag{26}$$

The second is a shark-tooth phase distribution given by the piecewise linear function

$$\Phi(r) = \begin{cases} \beta r & 0 \le r \le 0.5 \\ \beta r - 0.5\beta & 0.5 \le r \le 1\,. \end{cases} \tag{27}$$

Such phase distributions are characteristics of the phase error distributions that would be in the aperture of a RWPFAA when the guide is divided into two concentric sections, circular and annular, of *equal* radial lengths, each excited in proper phase. Schemes of two RWPFAAs of this type are shown in Fig. 11. For the RWPFAA shown in Fig. 11(a) the frequency-dependent phase error distribution would be saw-tooth, while for the one shown in Fig. 11(b) the frequency-dependent phase error distribution would be shark-tooth. Note that in these cases, the maximum phase in the circular aperture, for a given β, is only half that of the conical phase. Based on (26) and (27), the space factor of the circular aperture with uniform amplitude distribution and regularly serrated phase distributions can be written for the saw-tooth phase distribution as

$$SF(u) = 2\int_0^{0.5} \exp(j\beta r) J_0(ur) r\, dr + 2\exp(j\beta) \int_{0.5}^{1} \exp(-j\beta r) J_0(ur) r\, dr \tag{28}$$

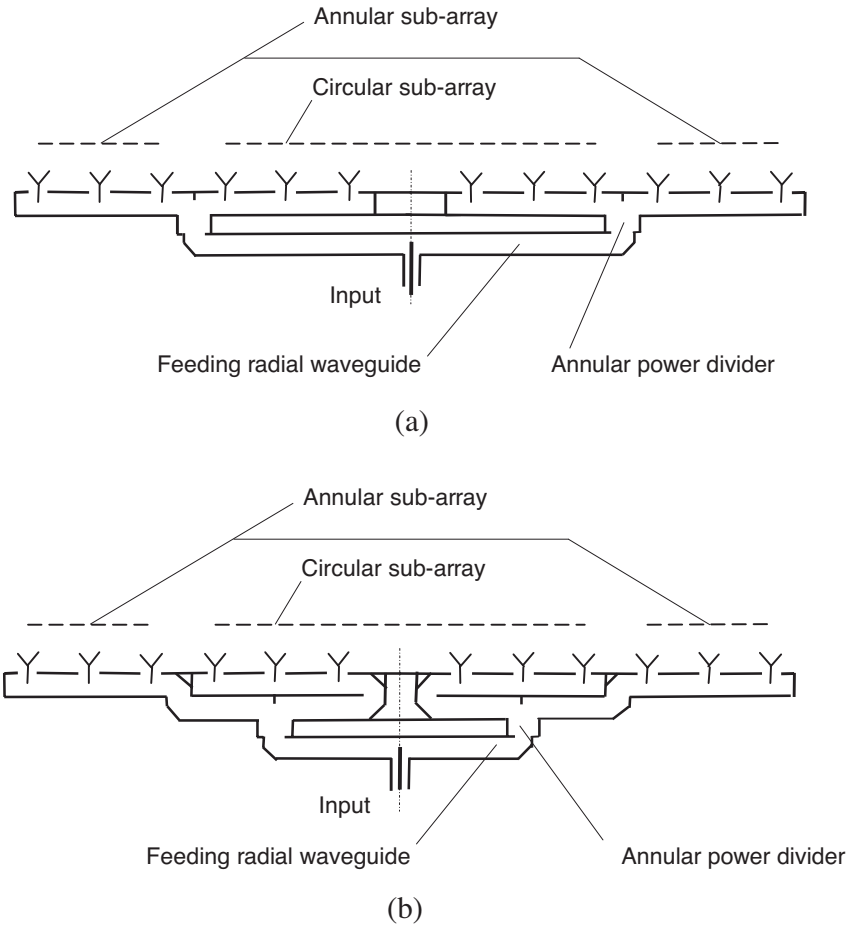

Figure 11. Schemes of two-section RWPFAAs in which the frequency-dependent aperture phase error distribution would be: (a) of a saw-tooth shape, (b) of a shark-tooth shape.

and for the shark-tooth phase distribution as

$$SF(u) = 2\int_0^{0.5} \exp(j\beta r) J_0(ur) r\, dr + 2\exp(-j\beta/2)\int_{0.5}^{1} \exp(j\beta r) J_0(ur) r\, dr. \tag{29}$$

Two sets of plots of the normalized space factors obtained by carrying out the integration in (28) and (29) numerically are shown in

Fig. 12. They are for the same values of the phase constant β used in Section 2 for the line source models. The plots show that for both of the serrated phase distribution considered, the side-lobe levels do not increase much when the phase constant β increases. For $\beta \leq \pi$, the level of the relatively broad side-lobe that emerges is lower than that of the first side-lobe. The gain factors, given by the values the respective space factors in the broadside direction, are presented in Table 4. A comparison of Table 4 with Table 3 shows that the decrease in gain due to the phase error, for the a given β, is markedly less in the serrated phase case than in the conical phase case.

Table 4. Gain factor of the uniformly excited two-section circular aperture with regularly serrated phase distributions.

β		0	$\pi/4$	$\pi/2$	$3\pi/4$	π
g(dB)	Saw-tooth distribution	0	-0.06	-0.22	-0.51	-0.91
	Shark-tooth distribution	0	-0.05	-0.21	-0.46	-0.83

Now let us consider the effect of increasing the number of sections in the circular aperture to more than two on the space factor. When more sections are used, the frequency-dependent phase-error distribution would be, depending on the feeding structure used, serrated saw-tooth, shark-tooth, combined saw-shark-tooth, or combined shark-saw-tooth. A scheme of a three-section RWPFAA for which the frequency-dependent phase error distribution would be combined saw-shark-tooth is shown in Fig. 13. Plots of the space factor of a multi-sectional circular aperture for various types of phase distributions and values of β are shown in Fig. 14, Fig. 15 and Fig. 16 for two, three, and four sections, respectively. The results are compared against the performance standards of the FCC for the far side-lobe radiation suppression levels [8]. From these figures, it is clearly seen that the far side-lobe level decreases when the number of sections is increased. It is also observed that the FCC performance standards for category A are only satisfied for small values of β. The FCC performance standards for Category B can be satisfied for larger values of β. When four-sections are used, Category B is satisfied for all values of β. Also, it can be noted that the lowest level of far sidelobes is obtained in the case of the combined saw-shark-tooth serrated phase distribution. A scheme of an RWPFAA of this type is shown in Fig. 17. The values of the gain factors obtained for these cases are presented in Table 5. Note that for a given β, the values of the gain factor decreases when the number of sections is increased. It can be further seen that

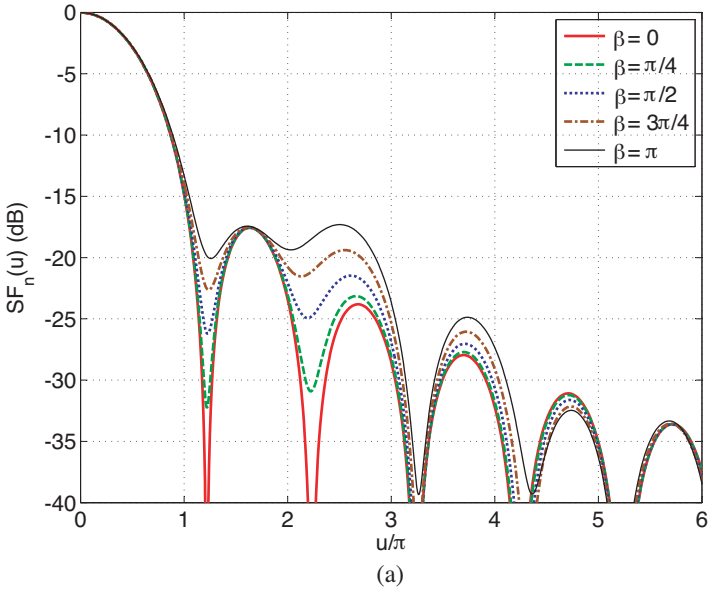

(a)

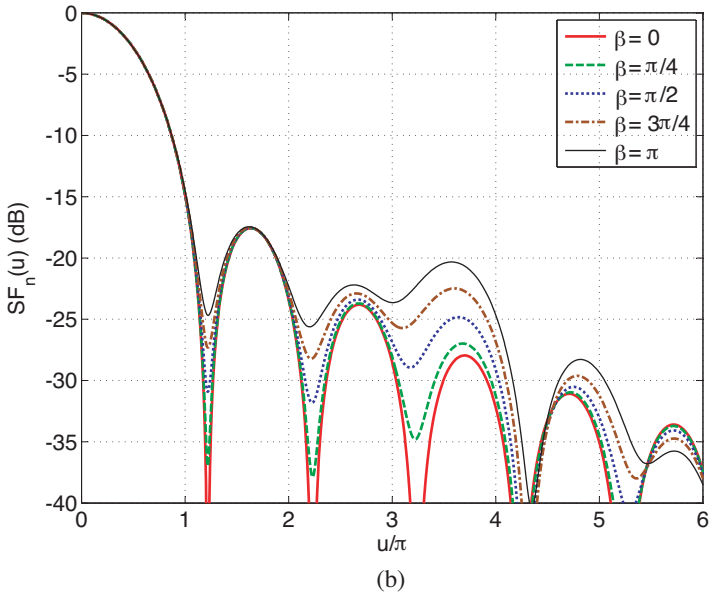

(b)

Figure 12. Plots of the normalized space factor of a circular aperture with uniform amplitude distribution and serrated phase distribution for different values of the phase constant β: (a) saw-tooth phase distribution; (b) shark-tooth phase distribution.

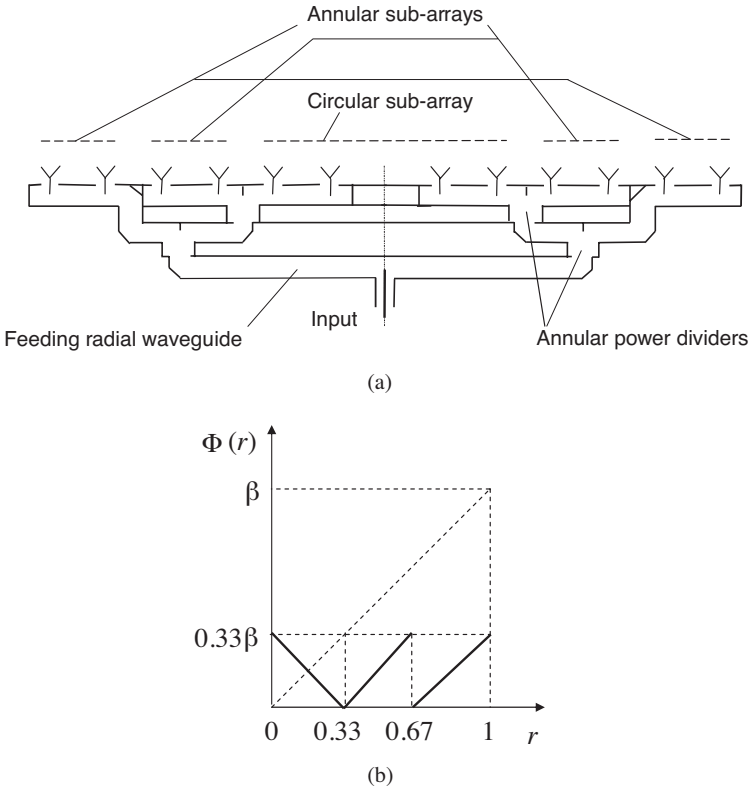

Figure 13. (a) Scheme of a three-section RWPFAA in which the frequency-dependent combined serrated aperture phase error distribution would be of a combined saw-shark-tooth shape. (b) Combined saw-shark-tooth phase distribution along the circular aperture radius.

the loss in gain in all cases is quite moderate, becoming even less than 1 dB for all values of β in the case of the four sections.

3.3. Circular Aperture with an Irregularly Serrated Phase Distribution

We now turn to the case of a circular aperture with uniform amplitude distribution and irregularly serrated phase distribution. Specifically, we consider a two-section circular aperture model, as before, but assume that the lengths of the two sections need not be equal. Two examples of irregularly serrated phase distributions are shown in

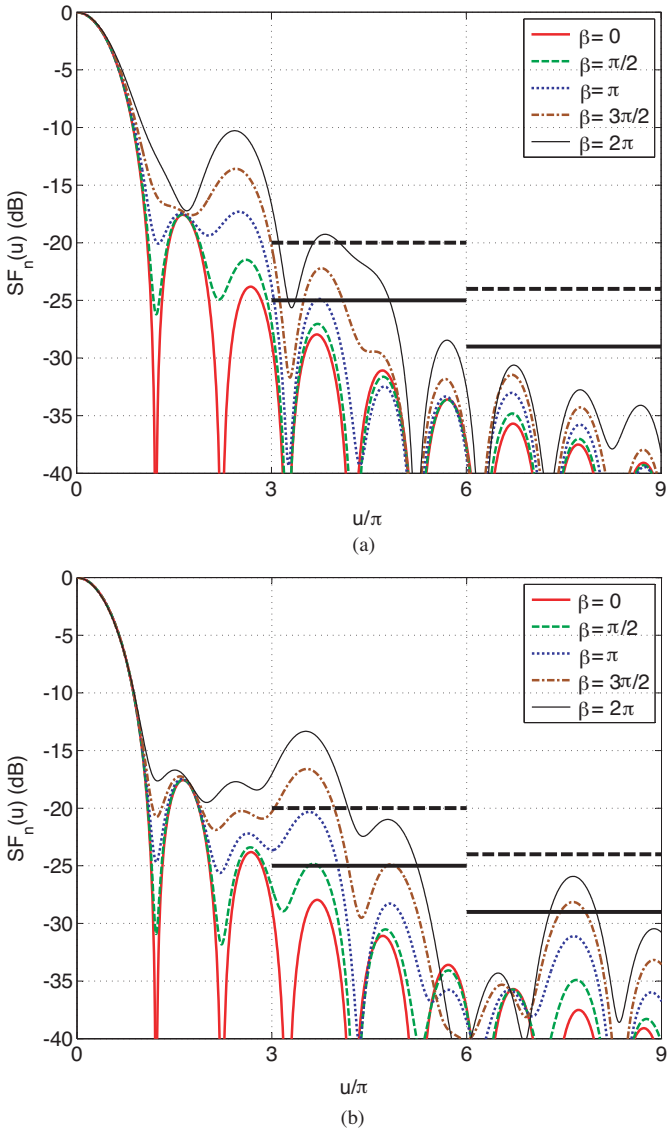

Figure 14. Plots of the normalized space factor of a two-section circular aperture with uniform amplitude distribution and serrated phase distribution for different values of the phase constant β: (a) saw-tooth phase distribution; (b) shark-tooth phase distribution. FCC requirements are shown by a thick solid line for category A, and by a thick dashed line for category B.

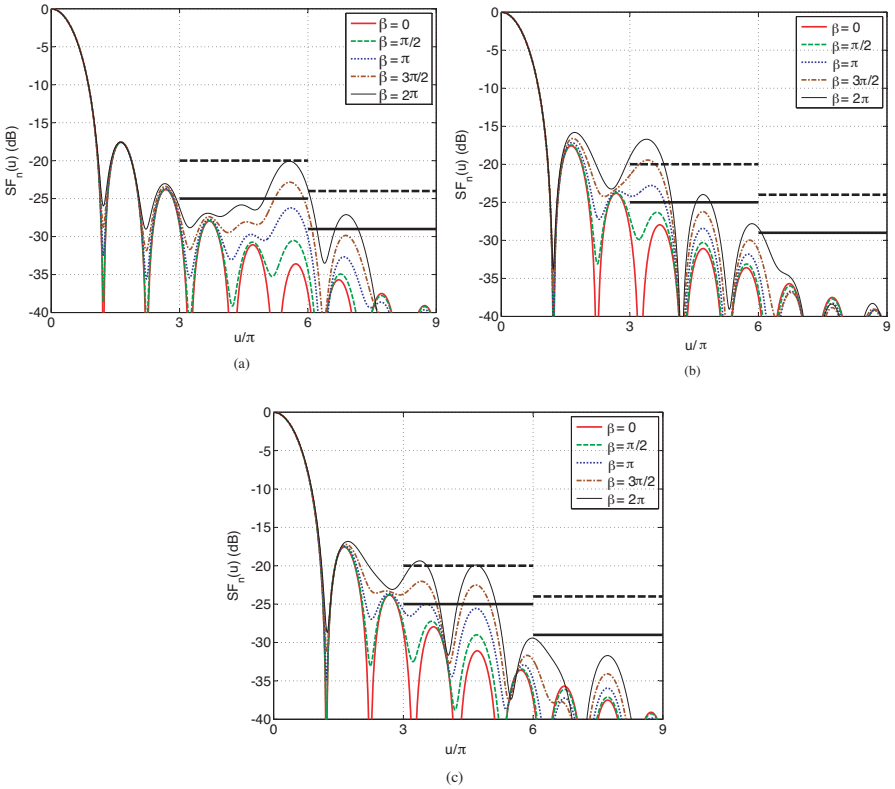

Figure 15. Plots of the normalized space factor of a three-section circular aperture with uniform amplitude distribution and serrated phase distribution for different values of the phase constant β: (a) shark-tooth phase distribution; (b) combined saw-shark-tooth phase distribution, (c) combined shark-saw-tooth phase distribution. FCC requirements are shown by a thick solid line for category A, and by a thick dashed line for category B.

Fig. 18. The first is an irregular saw-tooth phase distribution given by

$$\Phi(r) = \begin{cases} \beta r & 0 \le r \le r_1 \\ -\beta r + 2r_1\beta & r_1 \le r \le 1\,. \end{cases} \tag{30}$$

The second is an irregular shark-tooth phase distribution given by

$$\Phi(r) = \begin{cases} \beta r & 0 \le r \le r_1 \\ \beta r - r_1\beta & r_1 \le r \le 1\,. \end{cases} \tag{31}$$

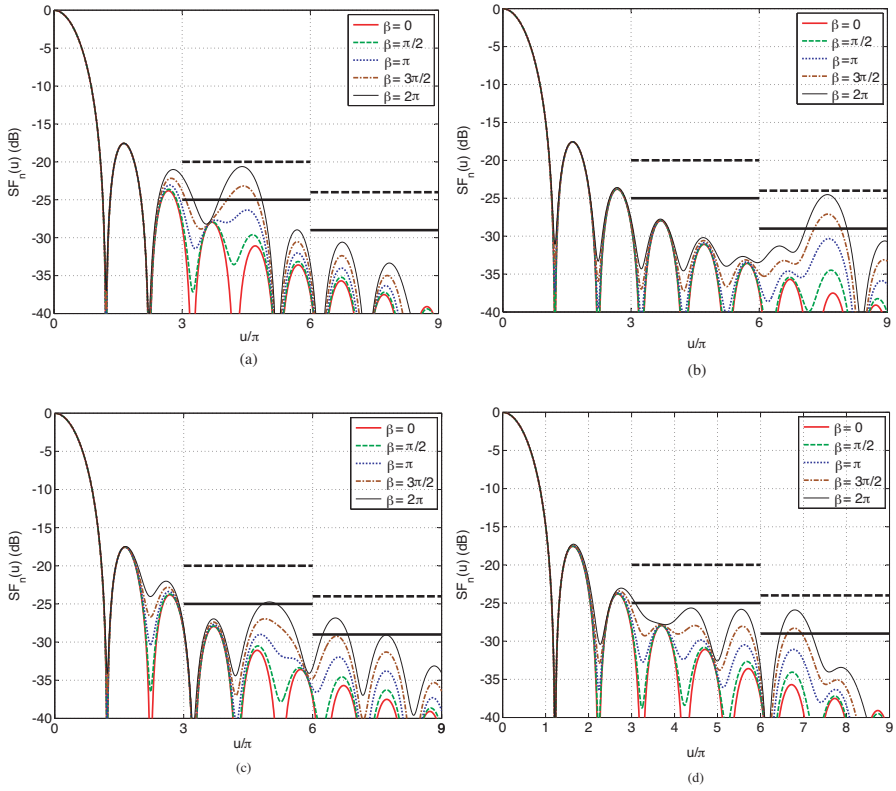

Figure 16. Plots of the normalized space factor of a four-section circular aperture with uniform amplitude distribution and serrated phase distribution for different values of the phase constant β: (a) saw-tooth phase distribution, (b) shark-tooth phase distribution, (c) combined saw-shark-tooth phase distribution, (d) combined shark-saw-tooth phase distribution. FCC requirements are shown by a thick solid line for category A, and by a thick dashed line for category B.

Here, r_1 is the radius of the first (circular) section. The space factor for the circular aperture with the irregular saw-tooth phase distribution can be written as

$$SF(u) = 2\int_0^{r_1} \exp(j\beta r) J_0(ur) r\, dr + 2\exp(2j\beta r_1) \int_{r_1}^{1} \exp(-j\beta r) J_0(ur) r\, dr, \tag{32}$$

Table 5. Gain factor for the multi-section circular aperture with regularly serrated phase error distribution.

Number of sections in the aperture	Type of the phase distribution	g (dB)				
		β				
		0	$\pi/2$	π	$3\pi/2$	2π
2	Saw	0	-0.22	-0.91	-2.11	-3.92
	Shark	0	-0.21	-0.83	-1.91	-3.50
3	Shark	0	-0.10	-0.39	-0.88	-1.58
	Saw-Shark	0	-0.10	-0.40	-0.90	-1.63
	Shark-Saw	0	-0.10	-0.40	-0.90	-1.65
4	Saw	0	-0.06	-0.22	-0.51	-0.91
	Shark	0	-0.05	-0.22	-0.50	-0.89
	Saw-Shark	0	-0.06	-0.22	-0.51	-0.91
	Shark-Saw	0	-0.06	-0.22	-0.51	-0.91

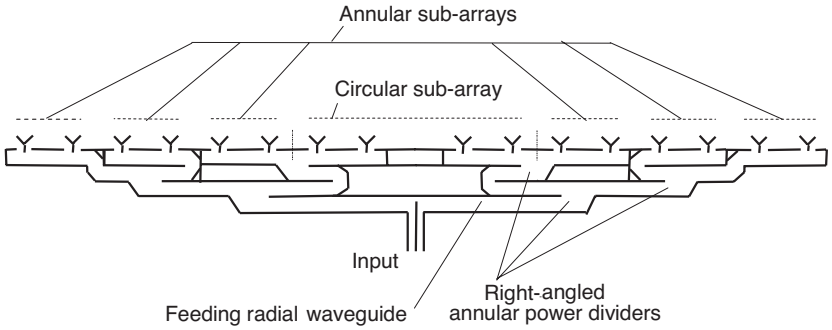

Figure 17. Scheme of a four-section RWPFAA in which the frequency-dependent aperture phase error distribution would be of a combined saw-shark-tooth shape.

and for the circular aperture with the irregular shark-tooth phase distribution as

$$SF(u) = 2\int_0^{r_1} \exp(j\beta r) J_0(ur) r\, dr + 2\exp(-j\beta r_1) \int_{r_1}^{1} \exp(j\beta r) J_0(ur) r\, dr\,. \tag{33}$$

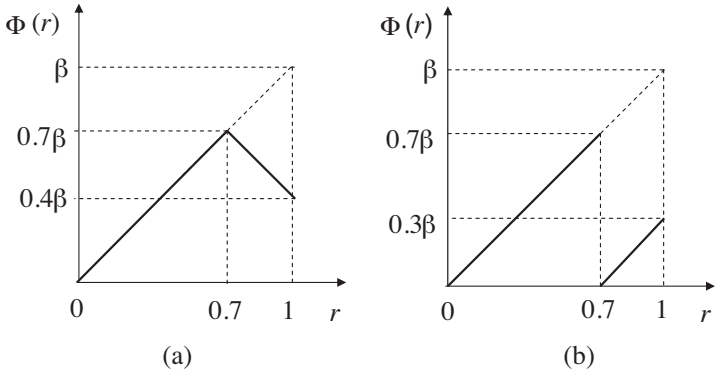

Figure 18. Irregular serrated phase distributions along the circular aperture radius for $r_1 = 0.7$: (a) saw-tooth phase distribution, (b) shark-tooth phase distribution.

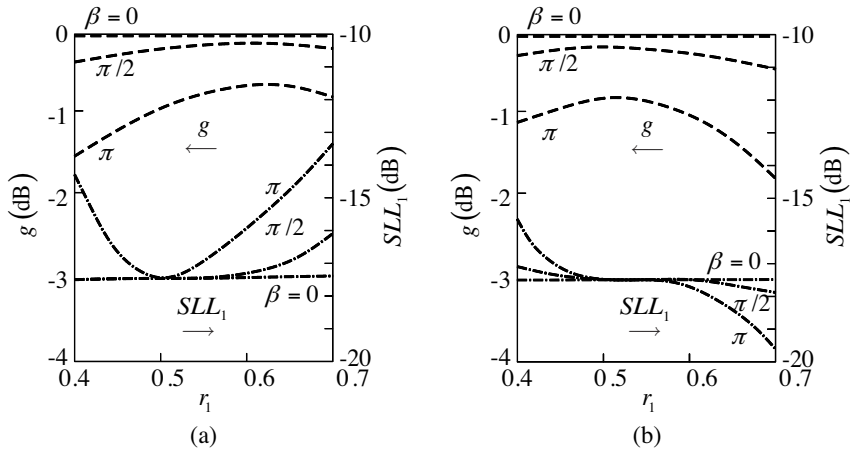

Figure 19. Gain and first side-lobe level of an aperture with a irregular serrated phase distribution: (a) saw-tooth phase distribution, (b) shark-tooth phase distribution.

Plots of the gain factor g and the first side-lobe level SLL_1 as functions of r_1 for the cases of the irregular saw-tooth and shark-tooth phase distributions are presented, respectively, in Fig. 19(a) and Fig. 19(b). As can be seen in Fig. 19(a), when $r_1 = 0.62$, the gain factor g reaches a maximum value of -0.67 dB, which agrees with the experimental value found in [10]. Note that this gain factor is slightly higher than the gain factor of -0.91 dB attained for $r_1 = 0.5$, which corresponds to

the case of regular phase distribution. Also note that for $r_1 > 0.5$ the level of the first sidelobe in the case of the irregular saw-tooth phase distribution increases with r_1. This is in contrast to the case of the irregular shark-tooth phase distribution, shown in Fig. 19(b), where the level of the first sidelobe decreases with r_1.

4. CONCLUSION

The feasibility of broadening the bandwidth of RWPFAA in terms of gain factor and side-lobe level characteristics has been studied. The idea is to render the frequency dependent phase error distribution in the aperture field serrated rather than conical. Models of a line source and a circular aperture radiating system with different types of the serrated phase error distribution have been considered. Three schematic designs of multi-section RWPFAAs that can provide broader frequency band of operation have been outlined. The radiating characteristics of some multi-section circular aperture antenna models have been compared against modern FCC performance standards.

REFERENCES

1. Carver, K. R., "A cavity-fed concentric ring phased array of helices for use in radio astronomy," Ph.D. Dissertation, University of Ohio, 1967.
2. Nakano, H., H. Takeda, Y. Kitamura, H. Mimaki, and J. Yamauchi, "Low-profile helical array antenna fed from a radial waveguide," *IEEE Trans. Antennas Propag.*, Vol. 40, No. 3, 279–284, 1992.
3. Nakano, H., S. Ikusawa, K. Ohishi, H. Mimaki, and J. Yamauchi, "A curl antenna," *IEEE Trans. Antennas Propag.*, Vol. 41, No. 11, 1570–1575, 1993.
4. Haneishi, M. and S. Saito, "Radiation properties of microstrip array antenna fed by radial line," *IEEE AP Symposium Digest*, 588–591, 1991.
5. Miyashita, H. and T. Katagi, "Radial line planar monopulse antenna," *IEEE Trans. Antennas Propag.*, Vol. 44, No. 8, 1158–1165, 1996.
6. Yamamoto, N., S. Saito, S. Morishita, and M. Haneishi, "Radiation properties of shaped beam antenna using radial line microstrip array," *IEEE AP Symposium Digest*, 1924–1927, 1996.
7. Shavit, R., L. Pazin, Y. Israeli, M. Sigalov, and Y. Leviatan, "Dual frequency and dual circular polarization microstrip nonresonant

array pin-fed from a radial line," *IEEE Trans. Antennas Propag.*, Vol. 53, No. 12, 3897–3905, 2003.

8. Federal Communications Commission Report and Order FCC 97-1, Jan. 1997.
9. Pazin, L. and Y. Leviatan, "Effect of amplitude tapering and frequency-dependent phase errors on radiating characteristics of radial waveguide fed non-resonant array antenna," *IEE Proc. Microw. Antennas Propag.*, Vol. 151, No. 4, 363–369, 2004.
10. Yamamoto, T., M. Takahashi, M. Ando, and N. Goto, "Enhancement of band-edge gain in radial line slot antennas using the power divider. A wide-band radial line slot antenna," *IEICE Trans. Commun.*, Vol. E78–B, No. 3, 1995.
11. Johnson, R. C., *Antenna Engineering Handbook*, 3rd edition, Chap. 4, McGraw-Hill, New York, 1993.